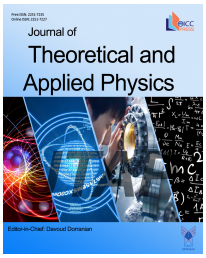

Volume 19, Issue 3, 192526 (1-15)

Journal of Theoretical and Applied Physics (JTAP)

https://doi.org/10.57647/j.jtap.2025.1903.26

Modeling magnetic fluid hyperthermia for tumors: A comprehensive study on skin tissue

Marziyeh Azad[1], Maliheh Ranjbaran[2,4,*], Sasan Soudi[3]

[1]*Department of Biology, CT.C, Islamic Azad University, Tehran, Iran.*
[2]*Department of Physics, CT.C, Islamic Azad University, Tehran, Iran.*
[3]*Department of Biomedical Engineering, CT.C, Islamic Azad University, Tehran, Iran.*
[4]*Institute of Biosocial and Quantum Science and Technologies, CT.C, Islamic Azad University, Tehran, Iran.*

[*]**Corresponding author:** ma.ranjbaran@iau.ac.ir

Original Research

Received:
8 May 2025
Revised:
11 June 2025
Accepted:
24 June 2025
Published online:
30 June 2025

Abstract:

Magnetic hyperthermia is a highly effective tumor therapy that utilizes the heat generated by activating magnetic nanoparticles with an alternating magnetic field. In this paper, to minimize the risk and optimize the therapy, we have conducted a simulation of magnetic heat generation in a three-layer skin medium with an elliptical tumor to treat skin cancer using the Fe_3O_4 magnetic nanoparticles. The model incorporates Darcy's Law and Brinkmann model, the transport of diluted species, and Pennes' bio-heat transfer equations within COMSOL Multiphysics software. The simulation accounts for the injection, diffusion, and induced heat generation of magnetic nanoparticles after exposure to a magnetic field. The simulation results show that the nanoparticles dispersed in the tumor after 24 hours, and the center of the tumor was destroyed after being exposed to the magnetic field with amplitude of 3.5 kA/m and frequency of 400 kHz for 1000 seconds. Also, the study investigated the effects of different temperature discretization methods, damage models, and temperature-dependent blood perfusion rates on tumor tissue damage. The results obtained from this study can provide valuable insights for optimizing various parameters of the thermotherapy procedure, such as exposure time, frequency and amplitude of applied magnetic field, and nanoparticles variables.

Keywords: Tumor treatment; Bio-heat transfer; Magnetic hyperthermia; Skin cancer; Magnetic nanoparticles; Computational modeling

1. Introduction

Cancer is a dangerous disease with no specific cause or definitive cure [1]. While chemotherapy is the most effective way to treat cancer, it does not guarantee a 100% success rate [2]. Ablative therapies, such as radiation therapy, can also cause cell damage. Unfortunately, these treatments often come with serious side effects, including hair loss, nausea, infertility, nerve damage, and general patient discomfort [3]. To address these challenges, hyperthermia has emerged as a potential therapeutic strategy for cancer treatment [4–6]. The goal of hyperthermia is to raise the temperature of the tumor to a sustained level above 42 °C [7]. This elevated temperature induces cancer cell death while minimizing damage to normal tissue [8, 9]. Hyperthermia offers the potential for non-invasive treatment with fewer side effects, making it an attractive approach for further research and development [10].

Hyperthermia can be generated using various irradiation methods, including ultrasound [11], radio frequencies [12], microwaves [13], infrared [14], lasers [15], and magnetic fields [16]. Among these methods, magnetic hyperthermia has shown efficiency in generating heat by utilizing magnetic nanoparticles (MNPs) in the presence of an alternating magnetic field (AMF). This approach involves delivering a liquid containing MNPs into the tumor and using a weak AMF to induce enough heat. To accurately predict the changes in temperature during magnetic hyperthermia therapy, it is important to develop reliable numerical models. These models can provide quantitative estimates of temperature distribution in the ferrofluid system. The reliability of the numerical model can be validated by comparing the temperature distribution obtained through experimental measurements with the results of the numerical analysis based on the finite element method [8, 17, 18].

Recent advancements in nanotechnology have contributed to the development of MNPs with various medical applications, including drug delivery [19], vascular imaging [20], and cancer therapy [21]. The synthesis of MNPs

can be achieved through different methods, including top-down (mostly physical) and bottom-up (mostly chemical) approaches [22].

Superparamagnetic iron oxide nanoparticles (SPIONs) such as magnetite Fe_3O_4 and maghemite γ-Fe_2O_3 are commonly used MNPs for injection into human tissues [23]. The heat dissipation mechanism in magnetic hyperthermia results from the energy loss caused by overcoming the rotational energy barrier under the AMF. The size of the superparamagnetic nanoparticles is smaller than the single-domain range, which means that under the AMF, the magnetization rotation must overcome the friction between the easy axis and the atomic lattice in the case of Neel relaxation, or between the MNP and its surroundings in the case of Brownian relaxation. Neel and Brownian relaxations result in the release of electromagnetic energy Losses which generate heat energy. The only difference between ferromagnetic and superparamagnetic single-domain NPs is that the latter randomly change the magnetization direction and are devoid of remanence and coercivity due to thermal fluctuations on the time scale of quasi-static magnetism measurements [24–26].

In addition to Fe_3O_4 nanoparticles, several other magnetic nanoparticles have been extensively investigated for magnetic fluid hyperthermia due to their superparamagnetic behavior, low toxicity, and thermal special properties. $CoFe_2O_4$ nanoparticles, for example, are more coercive and magnetically anisotropic than Fe_3O_4, which can lead to generation of greater heat under an alternating magnetic field [28, 29]. $MnFe_2O_4$ nanoparticles are also of interest in terms of their low toxicity, good biocompatibility, and tunable magnetic properties, which make them appropriate for biomedical applications [30]. Moreover, FePt nanoparticles are also found to have good thermal stability and high magnetic anisotropy, and hence superior specific absorption rate (SAR) performance, which is crucial for efficient tumor heating [31]. Nonetheless, $NiFe_2O_4$, despite being magnetically strong, increases biocompatibility concerns that may limit its clinical applications [30]. Though Fe_3O_4 is a well-established and biocompatible material, these other nanoparticles offer promising avenues for enhancing hyperthermia therapies and deserve more comparative research.

Computational modeling in the field of MNP hyperthermia is crucial for advancing the understanding, optimization, and safe implementation of this therapeutic modality. This approach allows researchers to simulate and predict the behavior of MNPs under the influence of an external alternating magnetic field (AMF) and assess their potential for therapeutic applications. Wang et al. [32] provides further insights into the significance and applications of mathematical modeling in this field. They evaluate the heat effects resulting from the dissipation of electromagnetic energy and the emission of thermal radiation from the ferrofluid system to the surrounding environment during the process of magnetic fluid hyperthermia. Manshadi et al. [33] developed a model of a four-layer structure of arterial tissue, considering porosity parameters and the interaction of particles with the tissue wall. Their findings indicated that increasing the size of particles/drugs/cargo enhances their retention in the tissue. Chanmugamet et al. [34]. presented a quantitative thermal analysis of breast cancer using a 3D computational model of the breast. By combining computational modeling with thermographic imaging and dynamic cooling, they demonstrated the potential of quantifying temperature distribution as an important tool for early breast cancer detection. Eagle et al. [35] utilized COMSOL Multiphysics software and the finite element method (FEM) to model a tumor as a sphere surrounded by normal tissue. They investigated nanoparticle heat production within the tumor under a weak magnetic field after the diffusion of nanoparticles. By monitoring the transient temperature profile of the tissue, they assessed the extent of damage to both the tumor tissue and the surrounding healthy tissue. These studies highlight the valuable role of computational modeling in optimizing magnetic hyperthermia treatments. By simulating the injection and diffusion of MNPs, as well as the thermal effects on tissue, these models contribute to improving treatment outcomes while minimizing risks. Suleman and colleagues [5] explored the use of magnetic nanoparticles for treating breast and brain tumors and found that stronger magnetic fields and frequencies led to higher tumor temperatures. Further investigations on the use of diluted nanoparticle solutions showed that tumor damage extent depended on heating duration and nanoparticle distribution within the tumor. They highlighted magnetic fluid hyperthermia (MFH) as a promising hypertherapeutic method targeting tumors specifically without harming surrounding normal tissues sensitive to heat [36].

The review of the literature highlights the need to investigate the effects of various factors on simulation of skin tumor tissue damage during magnetic fluid hyperthermia. This includes examining Darcy's Law and Brinkmann's model, different damage models, temperature discretization methods, and temperature-dependent blood perfusion rates, as well as optimizing procedure parameters like exposure time, frequency and amplitude of the applied magnetic field, and nanoparticle variables. So, in this study, we have proposed a modeling approach using the COMSOL Multiphysics package to investigate the treatment of skin tumors using magnetic hyperthermia. The goal is to optimize the procedure by studying the injection process, diffusion of magnetic nanoparticles (MNPs), and heat production. To model the skin tumor treatment, a three-layered human skin was represented using a two-dimensional, axisymmetric geometry. The model allows for the simulation of the injection process, where MNPs are introduced into the tumor region, and the subsequent diffusion of these particles. The heat production resulting from the interaction between the MNPs and the alternating magnetic field (AMF) is also included in the model. By varying parameters such as the AMF amplitude and frequency, nanoparticle concentration, maximum temperature, heating time, damage models, temperature discretization, and temperature-dependent blood perfusion rates, we aim to optimize the treatment by achieving an optimal extent of tissue necrosis while minimizing damage to healthy tissue. The COMSOL bio-heat model is a suitable tool for analyzing heat transfer in tissues and other living organisms. It provides a comprehensive solu-

tion for studying thermal effects in therapeutic applications. The integration of magnetic hyperthermia with bio-heat transfer modeling offers a novel approach to non-invasive and targeted skin cancer therapy. This combination has the potential to provide a more precise and effective treatment option, potentially reducing the need for more invasive procedures.

2. Simulation methods

The research involved creating a model of human skin with three layers: The epidermis, dermis, and subcutaneous tissue. Each layer had specified thicknesses of 0.05 mm, 1.20 mm, and 8.75 mm, respectively, from top to bottom. The tumor was approximated as an ellipse that spanned all three layers, measuring 2 mm in height and 5 mm in length. To simulate the skin model, a two-dimensional, axisymmetric geometry was employed in COMSOL Multiphysics®. The skin model was represented as a rectangular shape, with dimensions of 20 mm in length and 10 mm in height (as indicated in Fig. 1a and 1b). The injection of nanoparticles was performed using a 29-gauge needle [31].

In the simulation setup, the electromagnet is positioned parallel to the skin surface, allowing the magnetic field lines to pass through the skin and interact directly with the tumor. This configuration facilitates the targeted heating of the tumor region while minimizing damage to surrounding healthy tissue.

The bio-heat parameters for the modeled tissue, including the skin layers and the tumor, were documented in Table 1, as referenced in [4, 27].

After creating the geometry and defining the thermo-physical properties of the tumor and skin layers, the procedure of magnetic hyperthermia therapy was conducted in four steps.

Firstly, the nanoparticle fluid was injected into the tumor using Darcy's Law, which took approximately 15 minutes. Secondly, the dispersion of the nanoparticles into the tumor was allowed for approximately 24 hours, using the Transport of Diluted Species physics. Next, a magnetic field was activated for around 17 minutes, resulting in the transfer of heat from the magnetized nanoparticles to the tumor. Finally, once enough heat was transferred and the desired temperature for necrosis was achieved, the temperature was sustained for a period of time.

For an accurate calculation of the bio-heat transfer phenomenon from an engineering perspective, the time-dependent equation of Darcy's Law was utilized in the first step. The formulation of Darcy's Law is as follows:

$$\frac{\partial}{\partial t}(\rho\varepsilon_p) + \nabla\cdot(\rho\mathbf{u}) = 0 \tag{1}$$

$$\mathbf{u} = -\frac{k}{\mu}\nabla P \tag{2}$$

where ρ, ε_p, k and μ represent the nanoparticle fluid density, tumor porosity, tumor permeability, and nanoparticle fluid dynamic viscosity, respectively. The approximated fluid properties can be found in Table 2 and 3.

To establish the boundary conditions, the initial pressure value outside the regular tissue was assumed to be zero, as it was considered far enough from the nanoparticle injection

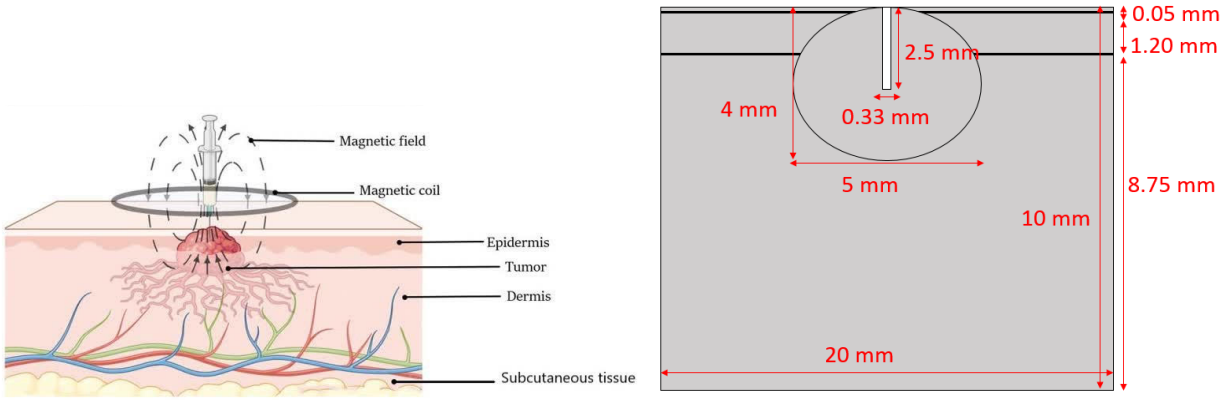

(a) (b)

Figure 1. (a) Schematic diagram of an ellipse tumor encased by normal tissue, with a needle for injection of nanoparticle fluid into the center of the tumor and an electromagnet to apply the magnetic field, (b) geometrical model of skin layers and tumor with specified dimensions.

Table 1. Symbols and thermo-physical properties of tumor and three layers of skin [4, 27].

	Density [kg/m^3]	Thermal conductivity [W/m·K]	Heat capacity [J/(kg·K)]	Blood perfusion rate [1/s]
Epidermis	1200	0.21	3598	0
Dermis	1000	0.37	3222	0.00125
Subcutaneous tissue	1000	0.16	2760	0.00125
Tumor	1100	0.55	4200	9.1×10^{-4}

Table 2. Parameters of Fe_3O_4 nanoparticles.

Parameter	Value	Ref.
Nanoparticle diameter	8 nm	[8, 37]
Nanoparticle density	5.24×10^6 [g·m^3]	[8, 37]
Nanoparticle heat capacity	670 [J/(kg·K)]	[8, 37]
Nanoparticle fluid dynamic viscosity	0.001 [pa/s]	[8, 37, 38]
Nanoparticle fluid viscosity	0.001 [pa·s]	[8, 37]
Magnetocrystalline anisotropy constant	9 [kJ/m^3]	[8, 37]
Average relaxation time in response to thermal fluctuation	10×10^{-9} [s]	[8, 37]
Domain magnetization	4.46×10^{-6} [Gauss]	[8, 39]

site. (Due to the minimal fluid flux out of the tumor tissue, the lymphatic pressure in the tumor domain was considered negligible. Therefore, we adopted a constant, near-zero value for lymphatic pressure in normal tissue, as reported in the literature [38, 41]). Additionally, due to symmetry, the pressure gradient beneath the needle injection site was set to zero. For all boundaries except the needle tip, no flow was taken into account. However, at the tip of the needle, an inward mass flux of 0.189 kg/(m^2·s) was applied to inject the nanoparticle fluid into the tumor. This mass flux was equivalent to a volume flow rate of 1 μL/min, with a fluid density of 1011.85 kg/m^3 and a needle tip area of a 29-gauge.

After the injection of MNPs, the mass transfer of nanoparticles into the tumor was modeled using the differential equation of the Transport of Diluted Species module. The equation is as follows:

$$\frac{\partial C_{NP}}{\partial t} + u_r \frac{\partial C_{NP}}{\partial r} + u_z \frac{\partial C_{NP}}{\partial z} = D_{NP,\text{tissue}} \left[\frac{1}{r} \left(\frac{\partial}{\partial r} r \frac{\partial C_{NP}}{\partial r} \right) + \frac{\partial^2 C_{NP}}{\partial Z^2} \right] \quad (3)$$

In this equation, C_{NP} represents the nanoparticle concentration, $D_{NP,\text{tissue}}$ is the diffusivity of nanoparticles through the tissue, and u is the convective speed profile. The parameter values used in the model can be found in Table 2 and 3.

Initially, it was assumed that there were no nanoparticles present in both the tumor and normal tissue, resulting in an initial concentration value of 0 g/m^3 (referred to as "eps" in COMSOL). Additionally, the flux value at the boundaries was assumed to be zero. This approach allows the analysis to primarily focus on understanding the behavior and distribution of heat within the tissue itself, specifically due to the internal heat source created by magnetic nanoparticles generating heat in magnetic hyperthermia. Fe_3O_4, the magnetic nanoparticle used in this project, has diameter of 8 nm and density of 5.24×10^6 g·m^3. The other parameters of these MNPs are reported in Table 2. All samples of Fe_3O_4 have the same morphology in the form of a sphere [42].

After the mass transfer of MNPs, a 24-hour diffusion period (or 86,400 seconds) could ensure effective dispersion. This diffusion period allows for the nanoparticles to spread and disperse evenly throughout the tissue, maximizing their potential for heat generation during magnetic hyperthermia [33].

The time-dependent heat transfer in the tissue was modeled using Pennes' bioheat equation:

$$\rho C_p \frac{\partial T}{\partial t} + \nabla \cdot (-k \nabla T) = Q_b + Q_{met} + Q_{ext} \quad (4)$$

In this equation, T represents temperature, ρ and C_p are the tissue density and specific heat, k is the thermal conductivity

Table 3. The parameters value used for heat transfer simulation of MNPs in the skin.

Parameter	Value	Ref.
Diffusivity of particles into tissue	2.5e^{-10} [m^2/s]	[8, 38]
Volumetric blood flow rate through tissue	5×10^{-4} [s^{-1}]	[8, 37]
Blood specific heat	3639 [J/kg·K]	[7, 8]
Blood density	1060 [kg/m^3]	[8, 40]
Arterial blood temperature	310.15 [k]	[8, 39]
Permeability of free space	$4\pi \times 10^{-7}$ [N/A^2]	[8, 37, 39]
Boltzmann constant	1.38×10^{-23} [J/K]	[8, 39]
Ligand layer thickness	1×10^{-9} m	[8, 37]

of the tissue. Q_b, Q_{met} and Q_{ext} are the blood perfusion term (bio-heat production), metabolic heat source, and external heat source (magnetic heat production by the nanoparticles), respectively. The blood perfusion term, which accounts for the effect of blood perfusion on temperature balance in the tissue, can be described by the following equation [26, 30]:

$$Q_b = \rho_b c_b \omega_m (T_\alpha - T) \tag{5}$$

Here, ρ_b is the blood density, c_b is the blood specific heat, ω_m is the blood perfusion rate, and T_α is the arterial blood temperature. The blood perfusion rate, ω_b, was modeled in different ways, all incorporating temperature dependence. In one model, it was considered quadratic with temperature, expressed as $\omega_b = \omega_0 + \gamma_0 T + \delta_0 T^2$, where $\omega_0 = 7 \times 10^{-4}$, $\gamma_0 = 1 \times 10^{-4}$, and $\delta_0 = 7 \times 10^{-6}$ [43]. Alternatively, a simple exponential relationship was proposed, where $\omega_b = \omega_0 \exp(0.0001T)$ with ω_0 representing a constant baseline perfusion rate [44]. This model suggests a consistent, gradual increase in blood perfusion with temperature.

The bio-heat transient process starts after the 24-hour diffusion of MNPs in the tissue. The power dissipation due to the distribution of MNPs in the tumor region when subjected to the AMF can be calculated using the equation [8, 30]:

$$Q_{ext} = \pi \mu_0 x_o H_o^2 f \frac{2\pi f \tau}{1 + (2\pi f \tau)^2} \tag{6}$$

In this equation, μ_0 is the vacuum magnetic permeability, x_o is the equilibrium susceptibility, H_o and f are the amplitude and frequency of the applied magnetic field, and τ is the effective relaxation time. Since, the Neel and Brownian processes take place in parallel, τ is given by the equation:

$$\tau^{-1} = \tau_N^{-1} + \tau_B^{-1} \tag{7}$$

Here, τ_N and τ_B are the Neel and Brownian relaxation times, respectively [8, 34].

Within the Bioheat Transfer module in COMSOL, the "Magnetic Heat Source" can be applied using the general source list under "Heat Source". The "Q_0" term, in this context, is equivalent to the Q_{ext}.

The parameter values used in the simulation of the flow and diffusion of MNPs in the tissue and tumor, as well as the bio-heat transfer calculations, are presented in Table 3.

The COMSOL Multiphysics package was used to couple Darcy's Law module, the transport of diluted species module, and the Bioheat transfer module. We also compared the results of Darcy's Law with Brinkmann' model. Brinkmann's equation, a more comprehensive version of Darcy's Law, is used to model fluid flow within porous tissue. The assumption of a higher viscous resistance at the fluid-solid interface than that within the fluid is valid only when the specific permeability k of porous media is low [45]. In Brinkmann equation:

$$\nabla \cdot \mathbf{u} = 0 \tag{8}$$

$$\left(\frac{\rho}{\varepsilon_P}\right)\frac{\partial \mathbf{u}}{\partial t} + \left(\frac{\mu}{k}\right)\mathbf{u} = -\nabla p + \nabla \cdot \left[\left(\frac{1}{\varepsilon_p}\right)\left(\mu(\nabla \mathbf{u} + (\nabla \mathbf{u})^T)\right)\right] + \mathbf{F} \tag{9}$$

ρ represents tissue density, $\mathbf{u}$ stands for flow velocity, κ indicates tissue permeability, p represents pressure, μ signifies dynamic viscosity, T denotes tissue temperature, ε_p indicates tissue porosity, and F represents the force caused by streaming [**?**].

This information is crucial for understanding the mechanisms behind this treatment approach and optimizing its effectiveness. This allowed for a 2D axial symmetry simulation, utilizing the parameter values from Table 2 and 3. The simulation aimed to investigate the fraction of necrotic tissue after heat transfer in the tumor.

3. Results and discussion

To numerically solve the coupled model presented in Fig. 2, we implemented an extremely fine mesh using the physically controlled mesh option based on the finite element method. This approach allowed us to accurately capture the details of the tissue-tumor structure and obtain precise results for the simulation.

In our method, we injected MNPs into the center of the tumor. The injection process lasted for 15 minutes (900 s) with a mass flow rate of 0.189 kg/(m^2·s). After that, the flow rate was gradually decreased to 0 kg/(m^2·s) over a period of 40 s. The streamline of Darcy's velocity field, which represents the flow velocity of the MNPs (in m/s), is depicted in Fig. 3. From the figure, we can observe that the velocity is highest at the injection site and gradually decreases as the MNPs move away from the tumor.

After the injection process, there is a high concentration of nanoparticles around the needle tip area. However, within minutes after injection, the nanoparticles become more dispersed throughout the tumor. To allow for enough dispersion of the nanoparticles within the tumor, a duration of 86400 seconds (24 hours) was specified for the diffusion process. This can be observed in Fig. 4, which shows the spatial distribution of nanoparticle concentration (in

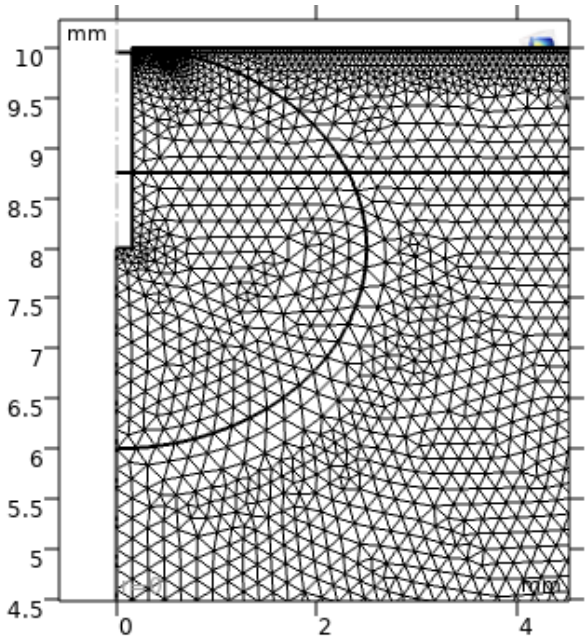

Figure 2. The mesh of the tissue-tumor structure.

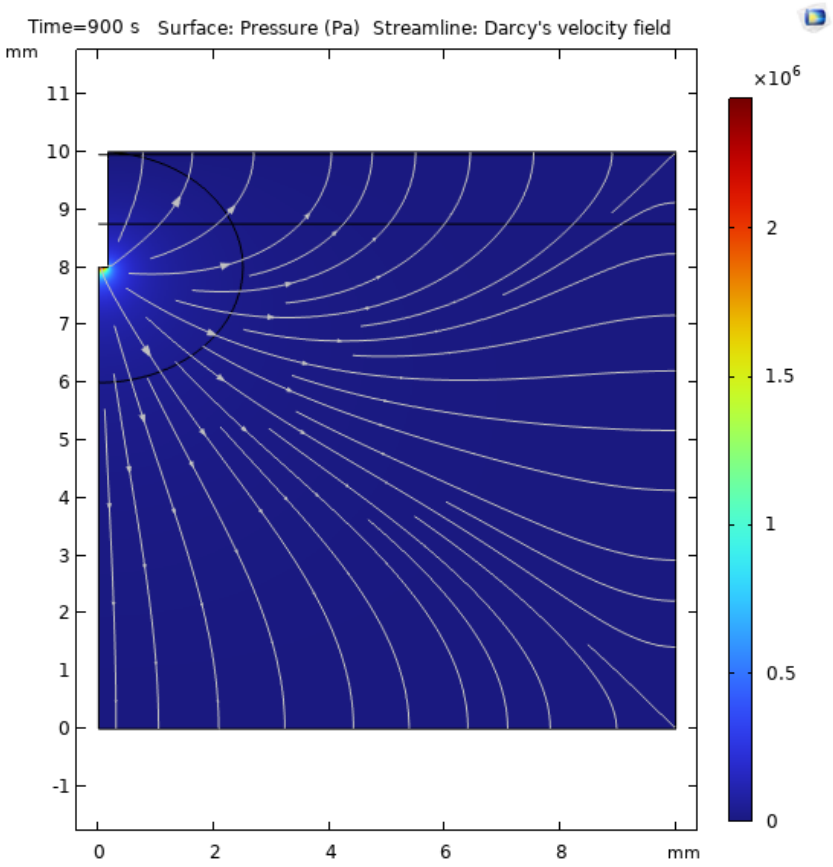

Figure 3. The Darcy's velocity field.

mol/m^3) within the tumor over the period of 0 to 24 hours. This extended period of diffusion ensures that the nanoparticles are evenly distributed throughout the tissue, allowing for a larger area of the tumor tissue to be heated during the subsequent heating process.

In Fig. 5b, the variation in MNPs concentration over time is shown at four points within the domain displayed in Fig. 5a. It is evident that the concentration of MNPs increases with time until it reaches a steady state level. Notably, the points that are closer to the injection site reach their highest concentration at the beginning of the injection process. On the other hand, the concentration of points that are further away from the injection site is lower compared to the points that are nearer. This observation suggests that the diffusion of MNPs is more effective in the immediate vicinity of the injection site, leading to higher concentrations in those areas.

After the 24-hour diffusion period, the tissue was subjected to an alternating magnetic field with an amplitude of 3.5 kA/m and a frequency of 400 kHz to generate heat for the treatment of cancerous tissue. In Fig. 6c, it is evident that the maximum temperature reached and the time taken to reach a steady state are different in the tumor and healthy tissue regions. The points nearest to the injection site reach higher temperatures in a shorter amount of time. This is because these points have a higher concentration of nanoparticles due to their proximity to the injection site. As a result, they absorb more energy from the alternating magnetic field and generate more heat, leading to higher temperatures.

As time progresses, the temperature within the tissue increases until the desired tissue reaches the desired temperature for necrosis. Fig. 6a-6c displays isothermal contours of the temperature field, which represent areas where the temperature remains constant. Contour lines connect points of equal temperature, while color gradients use different colors to indicate temperature variations.

These figures provide visual information about the heat transport and the uniform distribution of temperature within the tumor and the surrounding healthy tissue. The isothermal contours help to identify regions where the temperature reaches the desired level for effective treatment, ensuring that the tumor is adequately heated while minimizing damage to the surrounding healthy tissue.

In a successful cancer therapy method, it is crucial to control the temperature to effectively damage the cancerous tissue while minimizing injury to healthy tissue. Fig. 7 depicts a 3D graph of the temperature distribution in the modeled skin tissue resulting from heat therapy by the magnetic field. The temperature is highest at the needle tip and decreases with distance from the injection site.

As time progresses, the magnetically induced heat increases until it reaches the threshold temperature required for necrosis of the tumor tissue. If the temperature remains high enough (above 42 °C) for an enough duration, it will cause damage to the tumor, leading to its necrosis. As shown in Fig. 8, the inner part of the tumor reaches the maximum temperature, indicating that it experiences the highest level of damage. This observation suggests that the heat therapy method effectively targets and damages the tumor tissue,

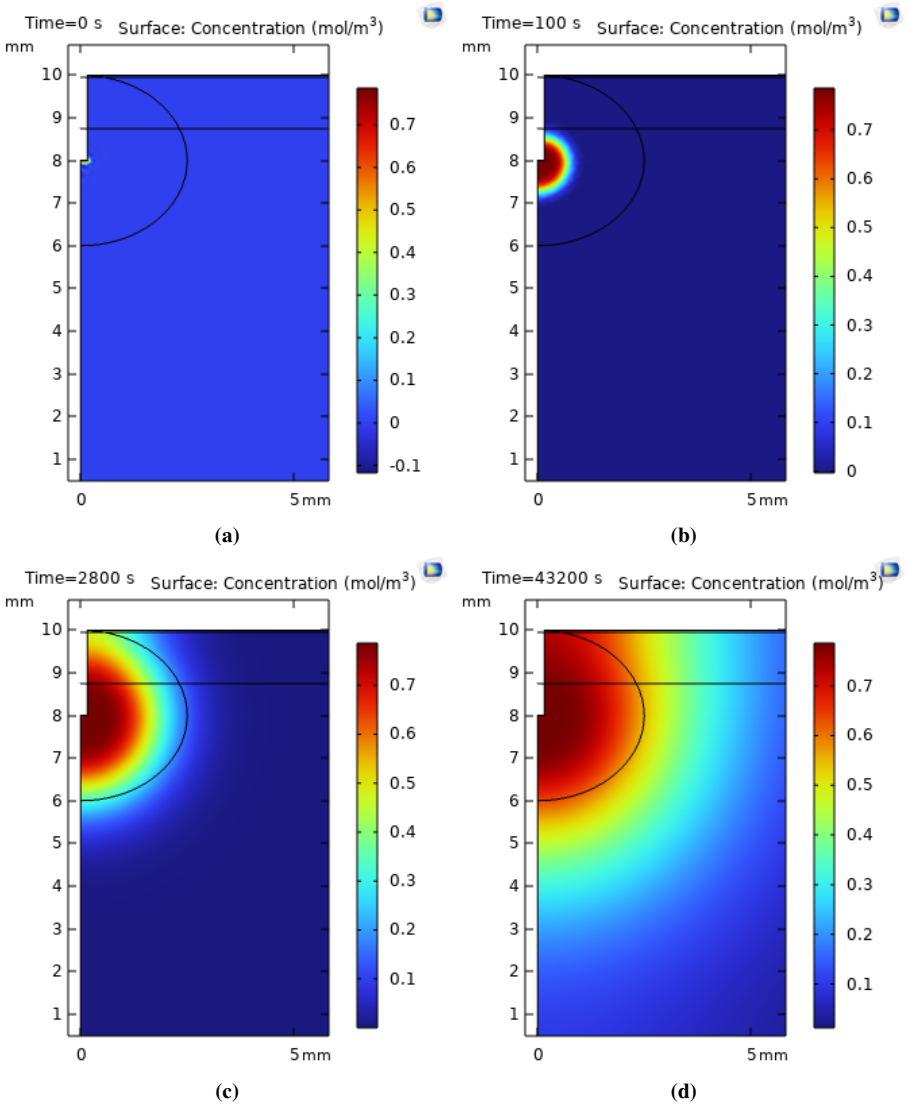

Figure 4. Change of nanoparticle concentration by increasing time at (a) 0 s, (b) 100 s, (c) 2800 s and (d) 86400 s.

while minimizing damage to the surrounding healthy tissue. The most characteristic and prevalent form of controlled cell death is called 'apoptosis', which originates from the Greek language. On the other hand, the uncontrolled form of cell death is commonly referred to as "necrosis". During necrosis, various pro-inflammatory proteins and compounds, such as NF-κ B, are up-regulated. This can lead to the rupture of cell membranes and the leakage of cellular contents into the

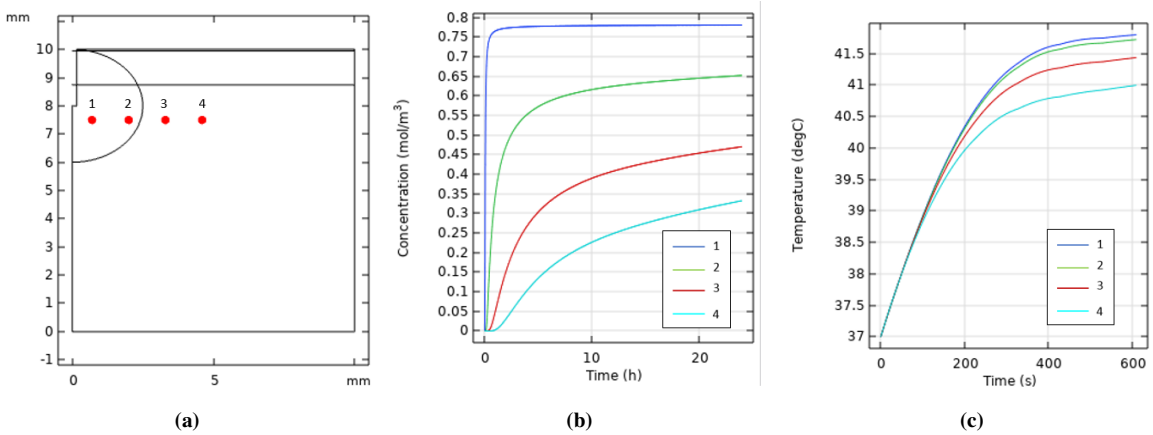

Figure 5. (a) Four cut points in tumor and healthy tissue (b) concentration variation at the four points, and (c) Temperature variation by time at the four points.

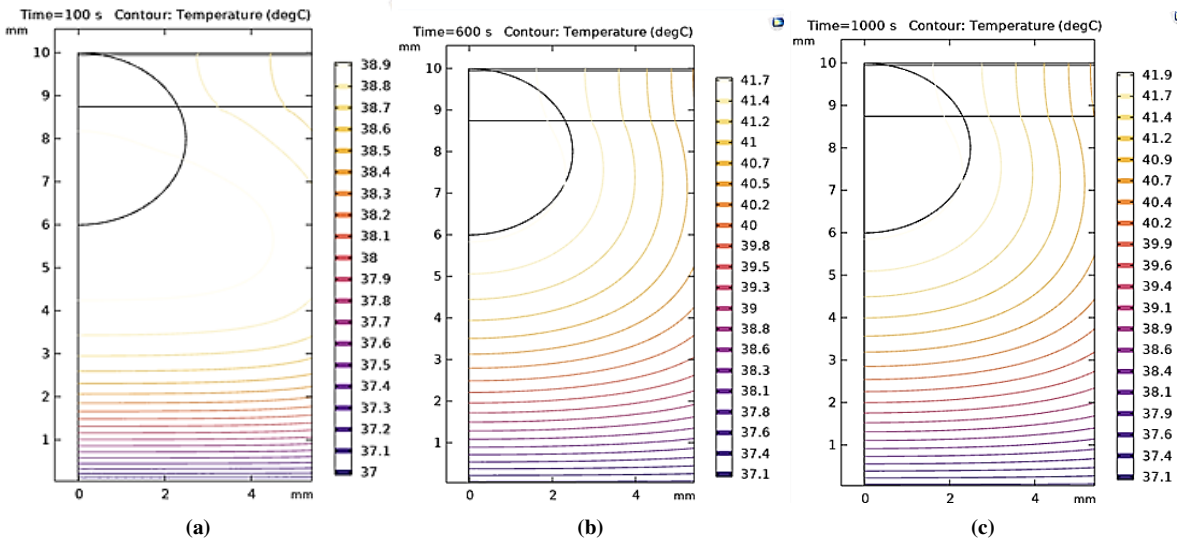

Figure 6. Contour diagram of temperature distribution by increasing time at (a) 100 s, (b) 600 s, and (c) 1000 s.

surrounding areas. Consequently, inflammation and tissue damage can occur [31].

In Fig. 8, a two-dimensional plot of the fraction of necrotic tissue in the magnetic heating process is depicted. It is evident that necrosis initiates faster near the needle tip. Although only a portion of the tissue is necrotic in this figure, we can conclude that the procedure is effective enough. Complete necrosis is observed only in the inner parts of

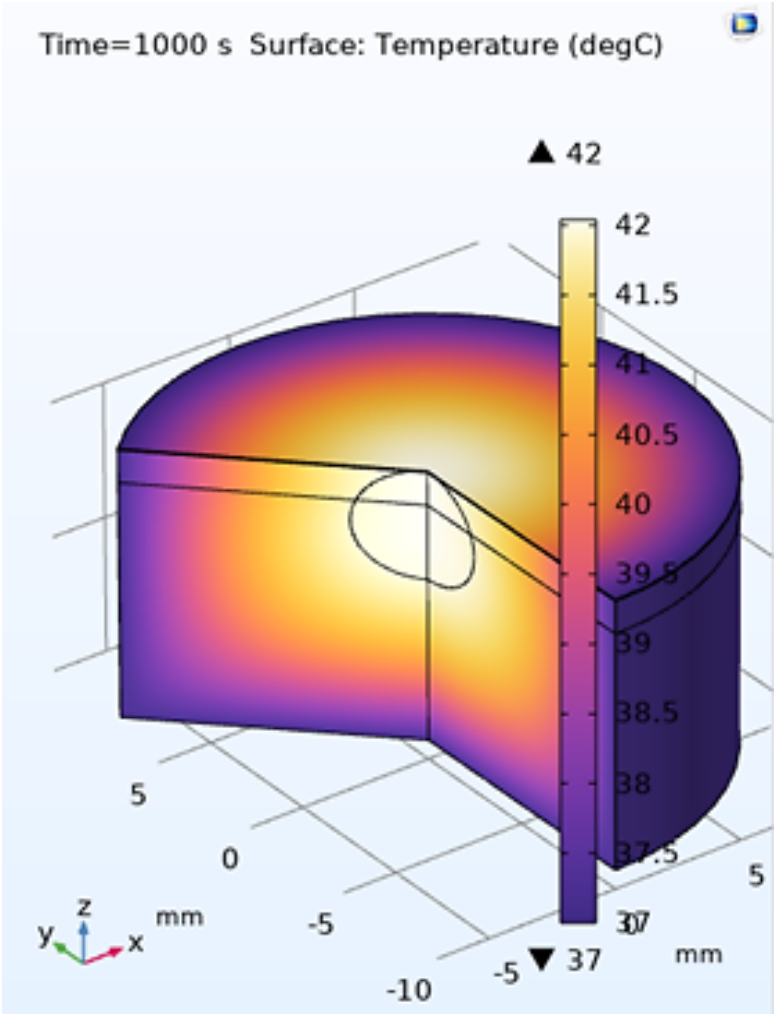

Figure 7. 3D graph of temperature distribution after 1000 seconds.

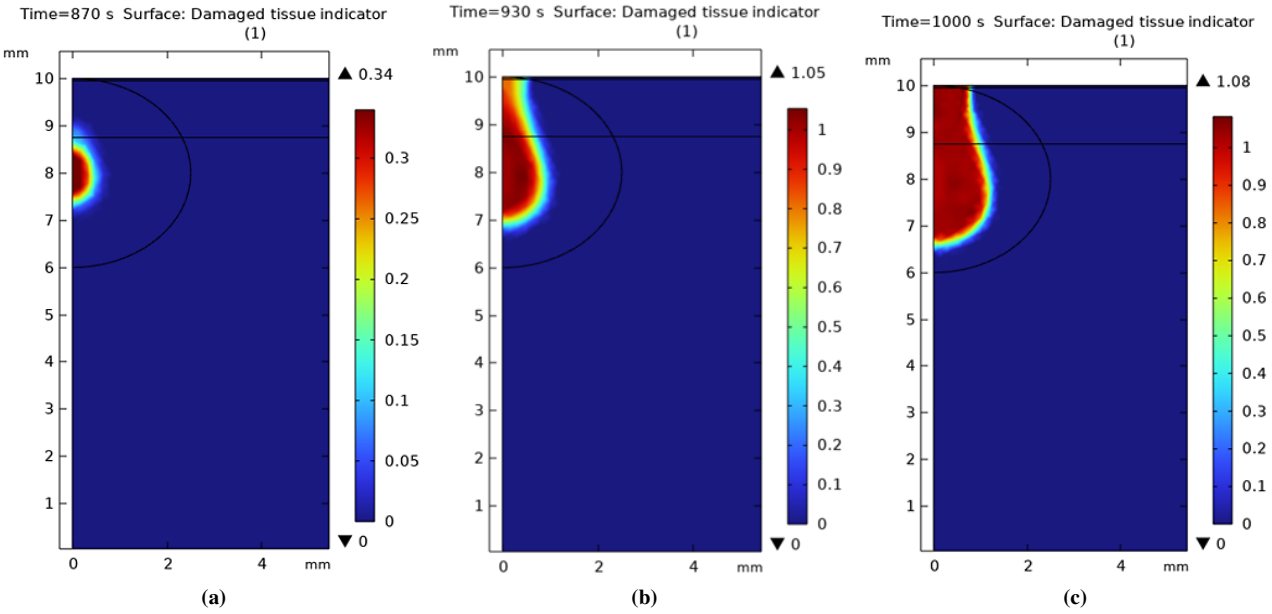

Figure 8. Two-dimensional plot of fraction of necrotic tissue in the magnetic heating process after, (a) 870 s, (b) 930 s, and (c) 1000 s.

the tumor, while other regions are damaged but not entirely necrotic. This technique effectively protects nearby normal tissues from damage, ensuring that they are minimally affected by the treatment.

To compare the results of Darcy's Law with Brinkmann model, Fig. 9 was depicted. This Figure demonstrates that the Brinkmann model yields a slightly higher temperature compared to Darcy's Law, albeit with a smaller slope. Consequently, this results in greater tumor damage through small fraction when utilizing the Brinkmann model.

In above simulations the blood perfusion rate was kept constant. However, Fig. 10 illustrates the 2D distribution of damaged tissue under two mentioned variable blood perfusion rate models [43, 44]. As shown, the fraction and overall amount of damaged tissue vary considerably among the models.

COMSOL Multiphysics offers a versatile tool for modeling thermal damage in biological tissues with its "Damaged Tissue Indicator" feature. This feature is defined by a shape function, with its discretization level playing a crucial role in the accuracy and computational cost of the simulation. Different discretization levels available in COMSOL include constant, linear, quadratic, cubic, quartic and quintic. Constant (default) is the simplest and fastest but least accurate, using a constant value within each element. Linear, quadratic, and cubic increase accuracy but also computa-

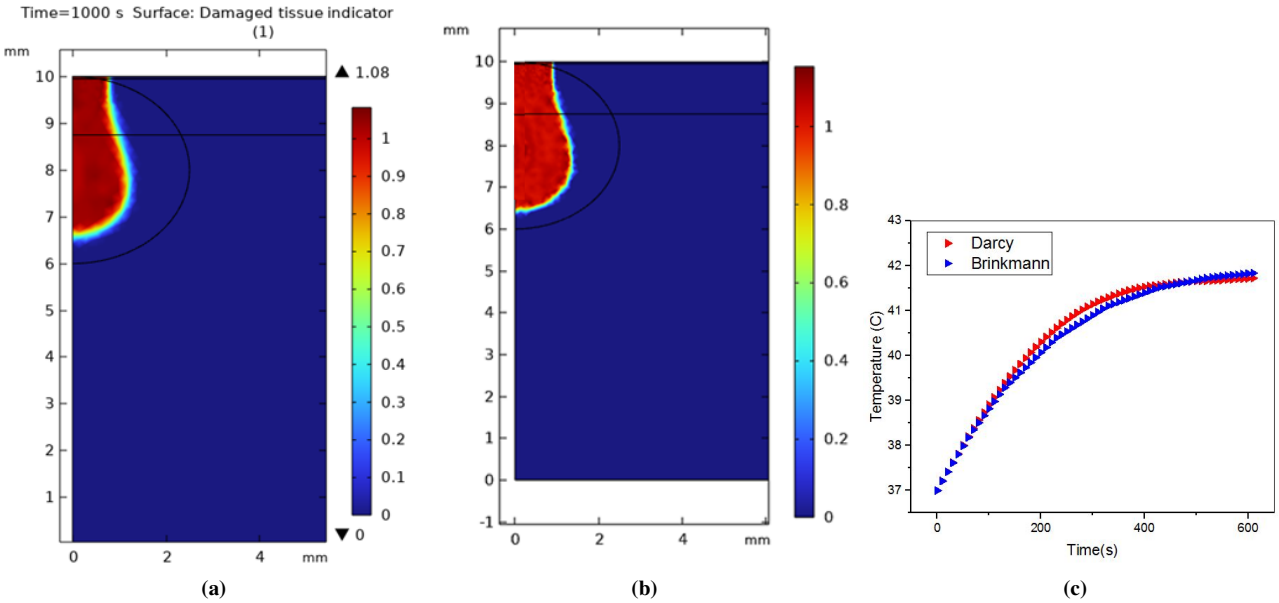

Figure 9. 2D representation of damaged tissue using (a) Darcy's Law, (b) Brinkmann model, and (c) comparison of temperature increase with time utilizing the two models.

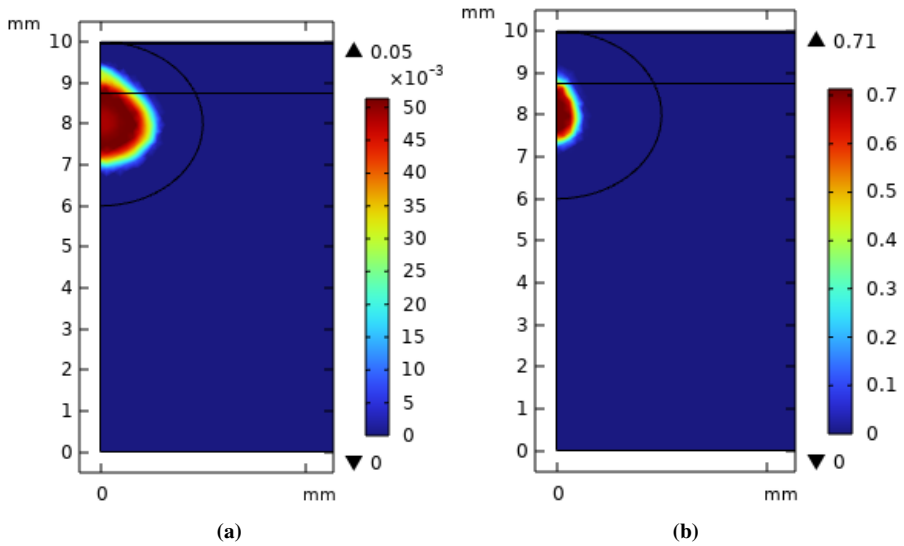

Figure 10. 2D representation of damaged tissue utilizing different blood perfusion rate (a) $\omega_b = \omega_0 + \gamma_0 T + \delta_0 T^2$, (b) $\omega_b = \omega_0 \exp(0.0001T)$.

tional cost by using increasingly complex functions within each element. Quartic and quintic, the higher-order approaches, further increase the accuracy by employing fourth and fifth-order polynomials, respectively. They offer the highest accuracy but are the most computationally expensive.

The choice of discretization level depends on the specific application and desired accuracy. For a general overview, Constant or linear models are sufficient, however, for intricate damage profiles, higher-order methods are preferable. Since there is minimal variation among the models in our simulation (as shown in Fig. 11), we have opted for the constant model.

When simulating heat transfer in COMSOL, we have the

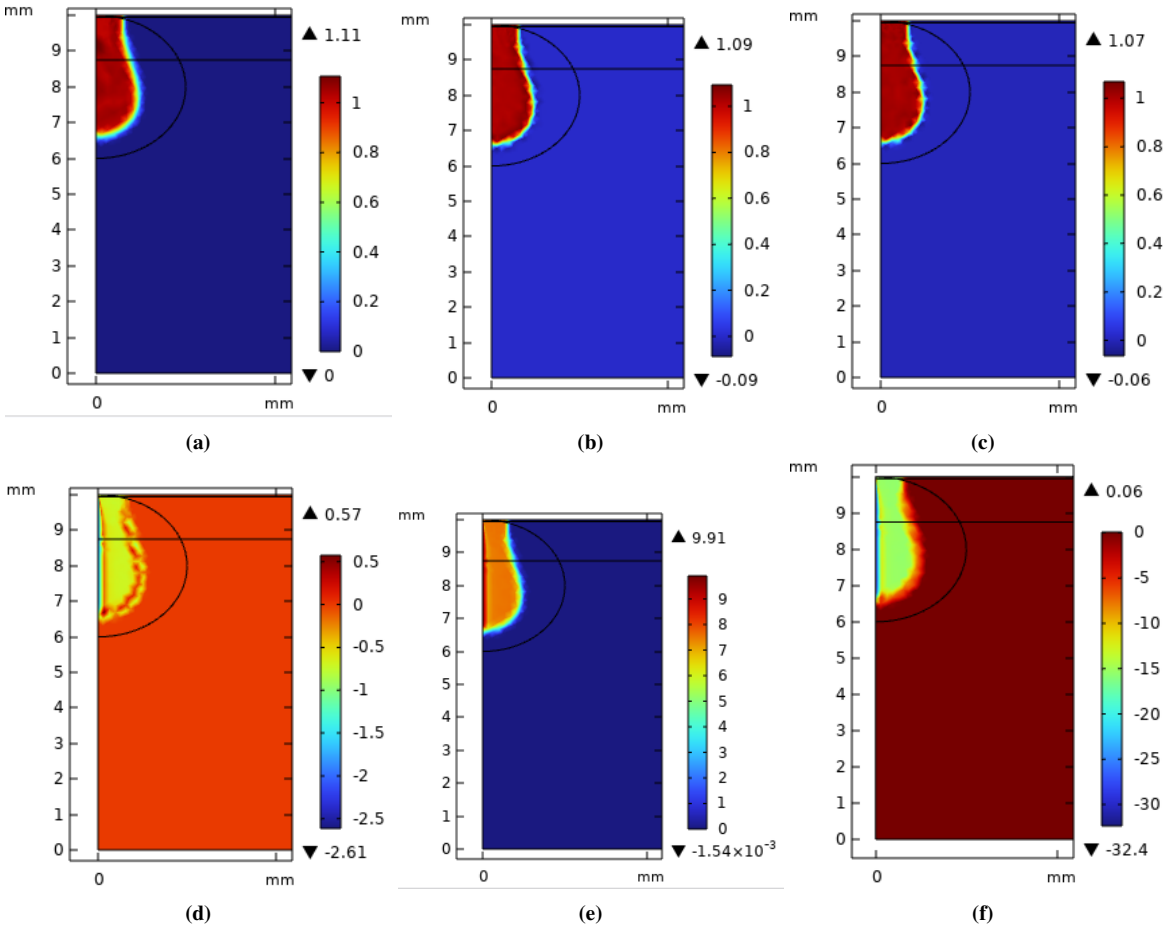

Figure 11. Different discretization levels of thermal damage (a) Constant, (b) Linear, (c) Quadratic, (d) Cubic, (e) Quartic, and (f) Quintic.

flexibility to adjust the precision of calculations by choosing a discretization order for the temperature field. This order, ranging from linear to quintic, determines the complexity of the function used to represent temperature within each element of the model. Furthermore, one can select between Lagrange or serendipity shape functions, which determine the type of interpolation used for representing temperature. Lagrange shape functions generally provide better accuracy in situations where elements are significantly distorted, particularly when compared to serendipity shape functions of the same order. As a default setting, COMSOL employs quadratic Lagrange shape functions when modeling heat transfer in solids. This choice strikes a balance between accuracy and computational efficiency for many common scenarios. Fig. 12 compares the extent of damaged tissue and temperature distribution for three different discretization methods: linear, quadratic Lagrange, and quartic Lagrange. As shown, increasing the discretization order from linear to quartic (both Lagrange and serendipity) results in only a very slight decrease in both damaged tissue and temperature.

To achieve effective cancer therapy within the desired time, it is crucial to accurately set the parameters to reach the desired temperature. The volumetric power dissipation, given by the equation $P = \mu_0 \pi \chi'' f H_0^2$, is directly related to the frequency (f) and the square of the amplitude of the alternating magnetic field (H_0). Therefore, by increasing the amplitude and frequency of the alternating magnetic field, the produced temperature can increase, and necrosis can approach the borders of the tumor and normal tissues. In this equation, χ'' represents the out-of-phase component of χ, which is related to the parameters of MNPs.

To investigate the effect of the amplitude of the alternating magnetic field on hyperthermia skin cancer treatment, an amplitude ranging from 3.5 to 4.5 kA/m was applied to the skin at a frequency of 400 kHz, and the resulting temperature was studied (Fig. 13).

The findings indicate that the temperature during hyperthermia skin cancer treatment rises until it reaches a maximum level, with the maximum temperature and the time taken to reach it being strongly influenced by the amplitude of the alternating magnetic field. Increasing the field amplitude leads to higher electromagnetic energy loss and thermal energy production, resulting in elevated temperatures during

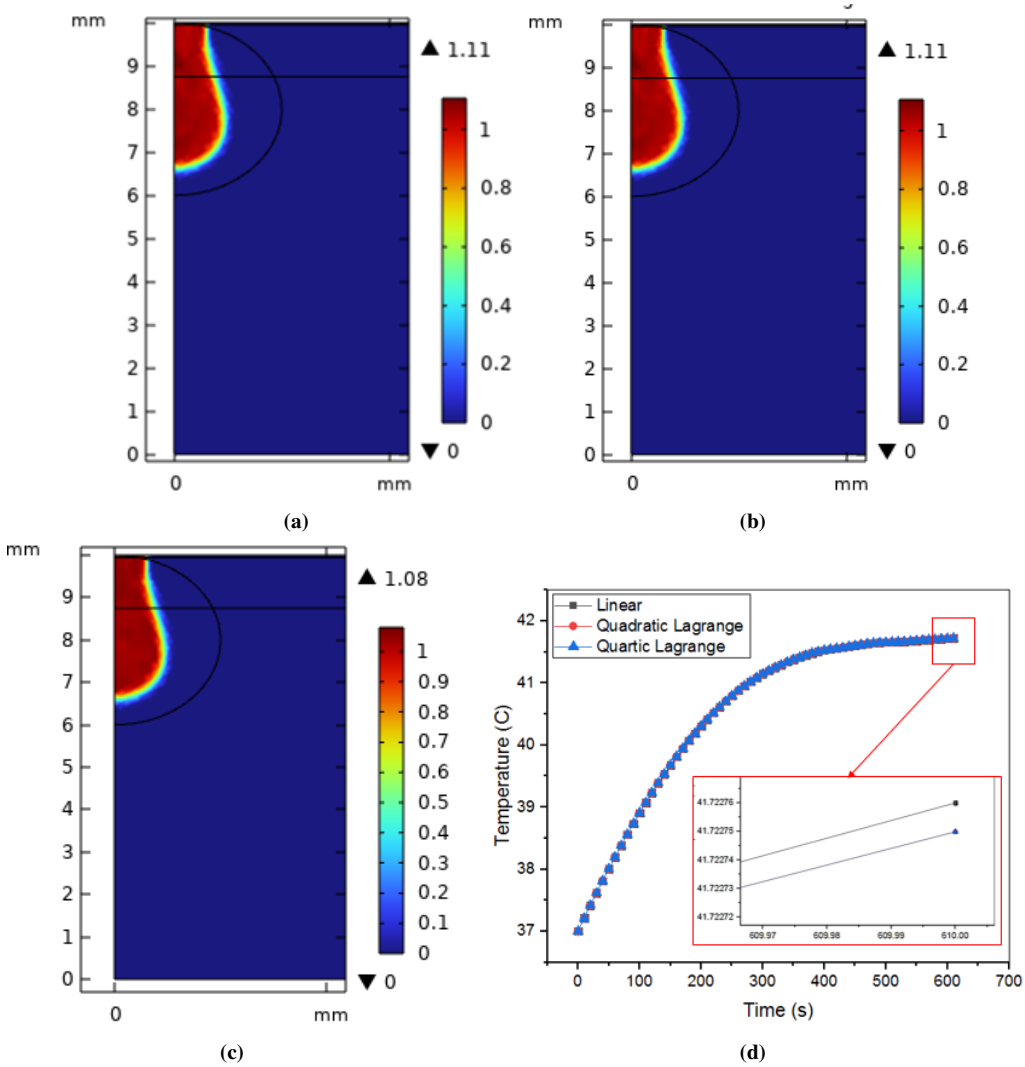

Figure 12. 2D damaged tissue after 1000 s while using (a) linear, (b) quadratic Lagrange, (c) quartic Lagrange temperature discretization orders, and (d) temperature variation at these discretization orders.

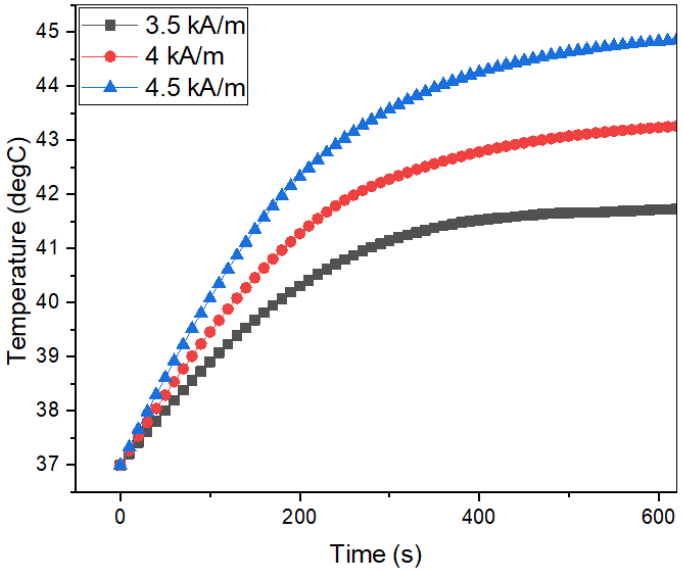

Figure 13. The produced temperature at three different AMF amplitudes and constant frequency of 400 kHz.

treatment. However, it is important to adhere to the recommended field amplitude of 7 kA/m for particles exhibiting superparamagnetic behavior to ensure biocompatibility and avoid potential negative effects. It is crucial to maintain the treatment parameters within the specified limits for the hyperthermia treatment of skin cancer to ensure safety and effectiveness [34]. Also, For safety reasons, clinical studies have shown that the product of magnetic field amplitude and magnetic field frequency should be kept below a value of approximately $C = 5 \times 10^9$ A/m·s [46]. The criterion in our study was 1.4×10^9 A/m.s for magnetic field with amplitude of 3.5 kA/m and frequency of 400 kHz.

The results presented in Fig. 14, displaying the temperature distribution at three different AMF frequencies, indicate that increasing the AMF frequency leads to higher maximum temperatures. This observation aligns with the understanding that magnetic heat dissipation is associated with the hysteresis loss of magnetic nanoparticles (MNPs). The hysteresis loss can be quantified by the equation $Q = \omega \cdot A \cdot f$, where ω represents the volume fraction of MNPs, A is the area of the hysteresis loop, and f is the frequency of the magnetic field.

The frequency of the magnetic field has a strong influence on the coercive field, which is the magnetic field required to demagnetize the MNPs. By controlling the coercive field through the choice of frequency, the dissipated heat and, consequently, the fraction of necrotic tissue can be effectively managed [32]. Therefore, selecting an appropriate AMF frequency can optimize the heat dissipation and enhance the effectiveness of the cancer treatment by promoting necrosis within the tumor. To ascertain the accuracy and reliability of the temperature-time profiles presented

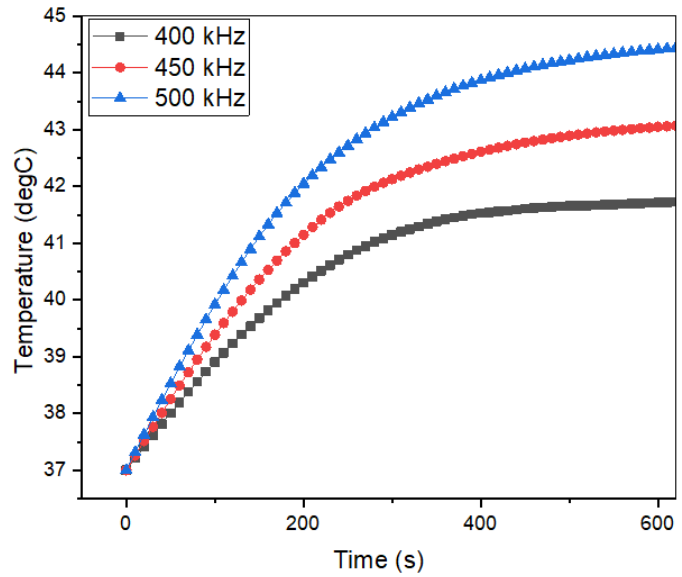

Figure 14. The produced temperature in tumor (second cut-point on Fig. 5a) at three frequencies of AMF and constant amplitude of 3.5 kA/m.

in Figures 12–14, we checked the model's numerical sensitivity to time-step and mesh size. A mesh independence test was implemented that confirmed temperature variations were within $1-2\%$ between the finer and coarser meshes. The volume fraction of MNPs, represented by ω, is determined by dividing the concentration of MNPs by their density. To analyze the impact of ω on the hyperthermia process, the inward mass flux in Darcy's Law was set to different values: 0.189, 0.945, and 1.89 kg/m^2·s, which correspond to volume flow rates of 1, 5, and 10 μL/min, respectively. Fig. 15 illustrates the consequences of increasing the mass flux. For higher concentrations, treatment should begin earlier than 24 hours, as the mass flux increases and the MNPs tend to leave the tumor area and diffuse into the surrounding healthy tissue. This diffusion can cause damage to the normal tissues surrounding the tumor. Also, lower flow rate may cause higher maximum temperature in tumor tissue [37]. So, the optimal distribution was achieved at a lowest flow rate of 1 μL/min, consistent with the findings of Darvishi et al. [7]. for higher concentrations, treatment should begin earlier than 24 hours.

Therefore, it is important to carefully consider the diffusion time and other magnetic parameters of the MNPs in order to achieve the best possible results. By optimizing these factors, the hyperthermia process can be controlled effectively, ensuring that the MNPs remain localized within the tumor and reduce damage to healthy tissues. This, in turn, can help in designing personalized treatment plans for individual patients, maximizing the therapeutic outcomes while minimizing adverse effects.

4. Conclusion

This study emphasizes the importance of simulating and analyzing the bio-heat transfer phenomena in magnetic hyperthermia therapy. We have utilized COMSOL Multiphysics software to investigate the magnetic heat generation in a three-layer skin medium with an elliptical tumor incorporating Fe_3O_4 nanoparticles and a comprehensive bio-heat transfer simulation. Our COMSOL Multiphysics model, incorporating Darcy's Law, the Brinkmann model, and Pennes' bio-heat equation, accurately predicted nanoparticle distribution and resulting tumor thermal damage. Simulations revealed complete tumor destruction at the center after 1000 seconds of exposure to a 3.5 kA/m, 400 kHz magnetic field, with minimal collateral damage to healthy tissue. Sensitivity analyses exploring various discretization methods, damage models, and perfusion rates further optimized treatment parameters.

The simulation results provide valuable insights for optimizing the thermotherapy procedure. The temperature distribution and fraction of necrotic tissue were investigated within the modeled skin tissue. The findings showed that necrosis initiates faster near the needle tip due to the higher concentration of MNPs in those areas. It was further shown that effective enhancement of bio-heat generation can be achieved by controlling the AMF amplitude and frequency, as well as the parameters of the MNPs. These findings have practical implications for optimizing magnetic hyperthermia treatment for various skin and tumor shapes. By exploring the potential of magnetic hyperthermia in skin cancer therapy, researchers can advance non-invasive and targeted treatment options, reducing risks associated with treatment and improving patient outcomes. This research has the potential to revolutionize cancer therapy by providing a less invasive alternative to traditional methods like surgery or radiation therapy.

Authors Contribution
M. A. and M. R. developed the theoretical formalism, performed the analytic calculations and numerical simulations. All authors provided critical feedback and helped shape the research, analysis and manuscript.

Availability of data and materials
The data that support the findings of this study are available from the corresponding author, upon reasonable request.

Conflict of interests
The authors declare that they have no known competing financial interests or personal relationships that could have appeared to influence the work reported in this paper.

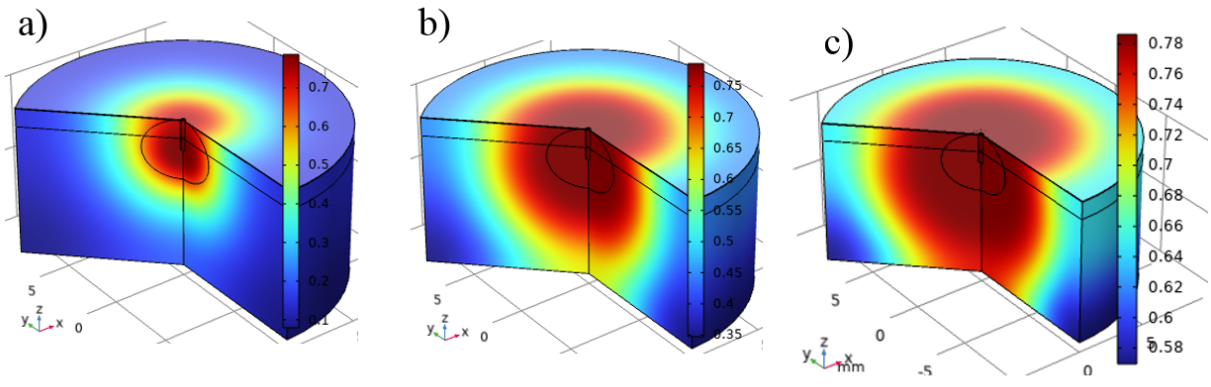

Figure 15. Concentration of MNPs in tumor and healthy tissue for inward volume flow rate of (a) 1 μL/min, (b) 5 μL/min, and (c) 10 μL/min after 24 hours.

References

[1] V. Darvishi, M. Navidbakhsh, and S. Amanpour. "Effects of temperature distribution in the tissue around the tumor on the quality of hyperthermia.". *2018 25th National and 3rd International Iranian Conference on Biomedical Engineering (ICBME)*, pages 1–6, 2018. DOI: https://doi.org/10.1109/ICBME.2018.8703501.

[2] K. Limsawan, P. Janpugdee, and F. C. Kunter. "Analysis of cancerous tissue temperature in the breast during hyperthermia.". *2017 International Symposium on Antennas and Propagation (ISAP)*, pages 1–2, 2017. DOI: https://doi.org/10.1109/ISANP.2017.8228868.

[3] J. Verma, S. Lal, and C. J. Van Noorden. "Nanoparticles for hyperthermic therapy: synthesis strategies and applications in glioblastoma.". *International Journal of Nanomedicine*, pages 2863–2877, 2014. DOI: https://doi.org/10.2147/IJN.S57501.

[4] S. Soni, H. Tyagi, R. A. Taylor, and A. Kumar. "Investigation on nanoparticle distribution for thermal ablation of a tumour subjected to nanoparticle assisted thermal therapy.". *Journal of Thermal Biology*, 43:70–80, 2014. DOI: https://doi.org/10.1016/j.jtherbio.2014.05.003.

[5] M. Suleman and S. Riaz. "3D in silico study of magnetic fluid hyperthermia of breast tumor using Fe_3O_4 magnetic nanoparticles.". *Journal of Thermal Biology*, 91:102635, 2020. DOI: https://doi.org/10.1016/j.jtherbio.2020.102635.

[6] A.-R. Tsiapla et al. "Mitigation of magnetic particle hyperthermia side effects by magnetic field controls.". *International Journal of Hyperthermia*, 38:511–522, 2021. DOI: https://doi.org/10.1080/02656736.2021.1899310.

[7] V. Darvishi, M. Navidbakhsh, and S. Amanpour. "Heat and mass transfer in the hyperthermia cancer treatment by magnetic nanoparticles.". *Heat and Mass Transfer*, 58:1029–1039, 2022. DOI: https://doi.org/10.1007/s00231-021-03161-3.

[8] S. Eagle, S. Wadsworth, and A. Wnorowski. "Modeling an injection profile of nanoparticles to optimize tumor treatment time with magnetic hyperthermia.". *BEE*, 2015.

[9] R. Rahpeima and C.-A. Lin. "Numerical study of magnetic hyperthermia ablation of breast tumor on an anatomically realistic breast phantom.". *PLOS ONE*, 17:e0274801, 2022. DOI: https://doi.org/10.1371/journal.pone.0274801.

[10] H. A. Elkayal, N. E. Ismail, and M. Lotfy. "Microwaves for breast cancer treatments.". *Alexandria Engineering Journal*, 54:1105–1113, 2015. DOI: https://doi.org/10.1016/j.aej.2015.06.012.

[11] J. Beik et al. "Measurements of nanoparticle-enhanced heating from 1 MHz ultrasound in solution and in mice bearing CT26 colon tumors.". *Journal of Thermal Biology*, 62:84–89, 2016. DOI: https://doi.org/10.1016/j.jtherbio.2016.10.007.

[12] J. H. Kim, E. W. Hahn, and P. P. Antich. "Radiofrequency hyperthermia for clinical cancer therapy.". *National Cancer Institute Monograph*, 61:339–342, 1982.

[13] F. Eltigani, S. Ahmed, M. Yahya, and M. Ahmed. "Modeling of interstitial microwave hyperthermia for hepatic tumors using floating sleeve antenna.". *Physical and Engineering Sciences in Medicine*, 45:569–575, 2022. DOI: https://doi.org/10.1007/s13246-022-01124-4.

[14] E. Kurgan and P. Gas. "Treatment of tumors located in the human thigh using RF hyperthermia.". *Przeglad Elektrotechniczny*, 87: 103–106, 2011.

[15] A. A. Elsherbini, M. Saber, M. Aggag, A. El-Shahawy, and H. A. Shokier. "Laser and radiofrequency-induced hyperthermia treatment via gold-coated magnetic nanocomposites.". *International Journal of Nanomedicine*, pages 2155–2165, 2011. DOI: https://doi.org/10.2147/IJN.S23952.

[16] R. R. Shah, T. P. Davis, A. L. Glover, D. E. Nikles, and C. S. Brazel. "Impact of magnetic field parameters and iron oxide nanoparticle properties on heat generation for use in magnetic hyperthermia.". *Journal of Magnetism and Magnetic Materials*, 387:96–106, 2015. DOI: https://doi.org/10.1016/j.jmmm.2015.03.085.

[17] J. L. Phillips. "A topical review of magnetic fluid hyperthermia.". *Journal of Science and Health at the University of Alabama*, 3:14–18, 2005.

[18] K.-C. Liu and P.-J. Cheng. "Numerical analysis of power dissipation requirement in magnetic hyperthermia problems.". *Journal of Thermal Biology*, 86:102430, 2019. DOI: https://doi.org/10.1016/j.jtherbio.2019.102430.

[19] H. Ahmad Panahi, S. Nourbakhsh, and F. Siami. "Synthesis of functionalized magnetic nanoparticles as a nanocarrier for targeted drug delivery.". *Advances in Polymer Technology*, 37:3659–3664, 2018. DOI: https://doi.org/10.1002/adv.22150.

[20] A. Soheilian, M. M. Tehranchi, and M. Ranjbaran. "Detection of magnetic tracers with Mx atomic magnetometer for application to blood velocimetry.". *Scientific Reports*, 11:7156, 2021. DOI: https://doi.org/10.1038/s41598-021-86358-0.

[21] I. Raouf, S. Khalid, A. Khan, J. Lee, H. S. Kim, and M.-H. Kim. "A review on numerical modeling for magnetic nanoparticle hyperthermia: Progress and challenges.". *Journal of Thermal Biology*, 91: 102644, 2020. DOI: https://doi.org/10.1016/j.jtherbio.2020.102644.

[22] M. Alavi and M. Rai. "Recent advances in antibacterial applications of metal nanoparticles (MNPs) and metal nanocomposites (MNCs) against multidrug-resistant (MDR) bacteria.". *Expert Review of Anti-infective Therapy*, 17:419–428, 2019. DOI: https://doi.org/10.1080/14787210.2019.1614914.

[23] P. Moroz, S. Jones, and B. Gray. "Magnetically mediated hyperthermia: current status and future directions.". *International Journal of Hyperthermia*, 18:267–284, 2002. DOI: https://doi.org/10.1080/02656730110108785.

[24] X. Liu et al. "Comprehensive understanding of magnetic hyperthermia for improving antitumor therapeutic efficacy.". *Theranostics*, 10: 3793, 2020. DOI: https://doi.org/10.7150/thno.40805.

[25] I. Raouf, P. Gas, and H. S. Kim. "Numerical investigation of ferrofluid preparation during in-vitro culture of cancer therapy for magnetic nanoparticle hyperthermia.". *Sensors*, 21:5545, 2021. DOI: https://doi.org/10.3390/s21165545.

[26] R. Ferrero et al. "Experimental and modelling analysis of the hyperthermia properties of iron oxide nanocubes.". *Nanomaterials*, 11: 2179, 2021. DOI: https://doi.org/10.3390/nano11092179.

[27] A. M. M. Mukaddes, M. R. Jaher, D. Roy, and R. Shioya. "A simulation study of bio-heat transfer in human skin under different burning conditions.". *AIP Conference Proceedings*, 1980:1, 2018. DOI: https://doi.org/10.1063/1.5044338.

[28] G. Goya, V. Grazu, and M. R. Ibarra. "Magnetic nanoparticles for cancer therapy.". *Current Nanoscience*, 4:1–16, 2008. DOI: https://doi.org/10.2174/157341308783591861.

[29] K. Heydaryan and M. Almasi Kashi. "Characterization and magnetic properties of $CoFe_2O_4$ nanoparticles synthesized under gas atmosphere: Effect of ferrofluid concentration on hyperthermia properties.". *Advanced Ceramics Progress*, 9:45–52, 2023. DOI: https://doi.org/10.1134/S1063784210110083.

[30] Y. A. Fahim, I. W. Hasani, and W. Mahmoud Ragab. "Promising biomedical applications using superparamagnetic nanoparticles.". *European Journal of Medical Research*, 30:441, 2025. DOI: https://doi.org/10.1186/s40001-025-02696-z.

[31] S. Maenosono and S. Saita. "Theoretical assessment of FePt nanoparticles as heating elements for magnetic hyperthermia.". *IEEE Transactions on Magnetics*, 42:1638–1642, 2006.
DOI: https://doi.org/10.1109/TMAG.2006.872198.

[32] I. Raouf, J. Lee, H. S. Kim, and M.-H. Kim. "Parametric investigations of magnetic nanoparticles hyperthermia in ferrofluid using finite element analysis.". *International Journal of Thermal Sciences*, 159:106604, 2021.
DOI: https://doi.org/10.1016/j.ijthermalsci.2020.106604.

[33] M. K. Manshadi et al. "Delivery of magnetic micro/nanoparticles and magnetic-based drug/cargo into arterial flow for targeted therapy.". *Drug Delivery*, 25:1963–1973, 2018.
DOI: https://doi.org/10.1080/10717544.2018.1497106.

[34] A. Chanmugam, R. Hatwar, and C. Herman. "Thermal analysis of cancerous breast model.". *ASME International Mechanical Engineering Congress and Exposition*, 45189:135–143, 2012.
DOI: https://doi.org/10.1115/IMECE2012-88244.

[35] S. Eagle, S. Wadsworth, and A. Wnorowski. "Modeling an injection profile of nanoparticles to optimize tumor treatment time with magnetic hyperthermia.". *BEE*, 2015.

[36] M. Suleman, S. Riaz, and R. Jalil. "A mathematical modeling approach toward magnetic fluid hyperthermia of cancer and unfolding heating mechanism.". *Journal of Thermal Analysis and Calorimetry*, 146:1193–1219, 2021.
DOI: https://doi.org/10.1007/s10973-020-10080-8.

[37] M. Javidi, M. Heydari, A. Karimi, M. Haghpanahi, M. Navidbakhsh, and A. Razmkon. "Evaluation of the effects of injection velocity and different gel concentrations on nanoparticles in hyperthermia therapy.". *Journal of Biomedical Physics & Engineering*, 4:151, 2014.

[38] M. Suleman and S. Riaz. "In silico study of hyperthermia treatment of liver cancer using core-shell $CoFe_2O_4$@$MnFe_2O_4$ magnetic nanoparticles.". *Journal of Magnetism and Magnetic Materials*, 498: 166143, 2020.
DOI: https://doi.org/10.1016/j.jmmm.2019.166143.

[39] Q. Jiang et al. "On the magnetic nanoparticle injection strategy for hyperthermia treatment.". *International Journal of Mechanical Sciences*, 235:107707, 2022.
DOI: https://doi.org/10.1016/j.ijmecsci.2022.107707.

[40] S. Ombelet et al. "Best practices of blood cultures in low-and middle-income countries.". *Frontiers in Medicine*, 6:131, 2019.
DOI: https://doi.org/10.3389/fmed.2019.00131.

[41] R. Van Leeuwen. "Development of an accurate temperature model for.". 2021.

[42] N. Mufti, D. Sari, A. Muyasaroh, and A. Taufiq. "Analyses of magnetic properties and crystal size on Fe_3O_4 nanoparticle from local iron sand using PEG as soft template.". *Journal of Physics: Conference Series*, 1595:012004, 2020.
DOI: https://doi.org/10.1088/1742-6596/1595/1/012004.

[43] E. Kengne, I. Mellal, M. B. Hamouda, and A. Lakhssassi. "A mathematical model to solve bio-heat transfer problems through a bio-heat transfer equation with quadratic temperature-dependent blood perfusion under a constant spatial heating on skin surface.". *Journal of Biomedical Science and Engineering*, 2014, 2014.
DOI: https://doi.org/10.4236/jbise.2014.79071.

[44] F. Ludin and S. Yahud. "Model of hyperthermia therapy in melanoma treatment: comparison between constant and temperature dependent blood perfusion rate.". *Journal of Telecommunication, Electronic and Computer Engineering (JTEC)*, 10:51–55, 2018.

[45] T. Wessapan and P. Rattanadecho. "Acoustic streaming effect on flow and heat transfer in porous tissue during exposure to focused ultrasound.". *Case Studies in Thermal Engineering*, 21:100670, 2020.
DOI: https://doi.org/10.1016/j.csite.2020.100670.

[46] R. Hergt and S. Dutz. "Magnetic particle hyperthermia—biophysical limitations of a visionary tumour therapy.". *Journal of Magnetism and Magnetic Materials*, 311:187–192, 2007.
DOI: https://doi.org/10.1016/j.jmmm.2006.10.1156.